Journal of Endocrinological Investigation
https://doi.org/10.1007/s40618-026-03033-9

ORIGINAL ARTICLE

Metabolic dysfunction-associated steatotic adrenal disease: a new entity in MetS, an experimental study in rabbits

Elena Rapizzi[1,2,3,6] · Lorenzo Zanatta[1,2,3] · Giulia Guarnieri[1] · Serena Martinelli[1] · Paolo Comeglio[4] · Gabriele Acciai[4] · Matilde Tavanti[1] · Sandra Filippi[5] · Letizia Canu[2,3,4] · Annamaria Morelli[1] · Mario Maggi[2,3,4]

Received: 4 March 2026 / Accepted: 19 August 2026

Abstract

Purpose High-fat diets (HFDs) are major drivers of metabolic alterations (obesity, insulin resistance, and hypertension). Although hypertension is a hallmark of metabolic syndrome (MetS), the involvement of adrenals remains underexplored. This study investigates the morpho-functional alterations of the adrenals in a rabbit model of HFD-induced MetS.

Methods Adult rabbits were fed either a regular diet (RD) or a high-fat diet (HFD) for 12 weeks. Adrenal glands were harvested for subsequent analysis. Morphological, histological, and immunohistochemical evaluations were conducted to determine steatosis, inflammation, fibrosis, and CYP21A2 distribution. Steroidogenesis was analysed through gene expression profiling and by measuring plasma steroid hormones.

Results HFD rabbits developed hallmark features of MetS. The adrenals glands of HFD rabbits were larger and showed marked lipid accumulation, macrophage infiltration, inflammation, and fibrosis. Concurrent with the presence of hypertension, HFD rabbits had significantly lower aldosterone levels and systemic downregulation of renin-angiotensin system genes. Steroidogenesis was also impaired, with reduced expression of key enzymes. However, mass spectrometry showed elevated plasma levels of progesterone and 11-deoxycorticosterone (11-DOC), suggesting a steroidogenic shift. CYP21A2 enzyme expression was altered, showing reduced presence in the zona glomerulosa but increased expression in the fasciculata. Finally, 11-DOC levels correlated positively with all MetS features.

Conclusion This study reveals that HFD causes significant structural changes in the adrenal glands within a MetS model. This structural damage could lead to a steroidogenic disarray that potentially drives hypertension through the accumulation of 11-DOC, independently of RAAS. These findings identify adrenal glands as active participants in MetS pathophysiology. We termed these alterations Metabolic Dysfunction-Associated Steatotic Adrenal Disease (MASAD).

Elena Rapizzi and Lorenzo Zanatta contributed equally to this work.

✉ Elena Rapizzi
elena.rapizzi@unifi.it

✉ Mario Maggi
mario.maggi@unifi.it

[1] Dept. Experimental and Clinical Medicine, University of Florence, Florence, Italy

[2] ENS@T Centre of Excellence, Florence, Italy

[3] Centro di Ricerca e Innovazione sulle Patologie Surrenaliche, AOU Careggi, Florence, Italy

[4] Dept. Experimental and Clinical Biomedical Sciences, University of Florence, Florence, Italy

[5] Interdepartmental Laboratory of Functional and Cellular Pharmacology of Reproduction, Department of Neurosciences, Psychology, Drug Research and Child Health (NEUROFARBA), University of Florence, Florence, Italy

[6] Viale Pieraccini 6, Firenze 50139, Italy

Published online: 26 August 2026

Graphical abstract

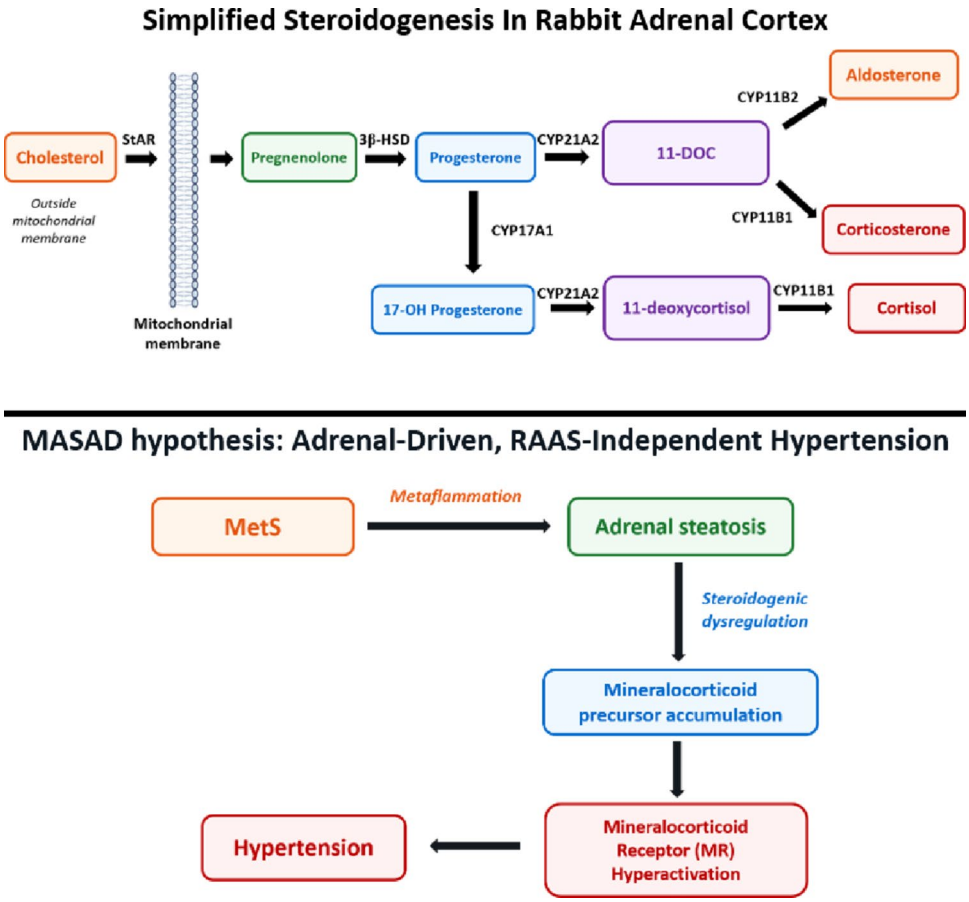

Keywords High fat diet · Metabolic syndrome · Adrenal glands · Inflammation · Fibrosis · Mineralocorticoids

Introduction

The lack of physical activity and the rise of westernised high-fat diets (HFDs) in modern lifestyles have significantly contributed to a global epidemic of non-communicable chronic disorders, including visceral obesity, insulin resistance, dyslipidaemia, and hypertension. This has led to an increased risk of diabetes and cardiovascular diseases (CVD) [1–3]. Accordingly, CVD is currently considered the leading cause of death alongside malignancies, while the global prevalence of diabetes doubled in the last 30 years [4]. Metabolic syndrome (MetS) is defined as a combination of metabolic abnormalities including: insulin resistance (impaired glucose tolerance, and type 2 diabetes mellitus), dyslipidaemia (characterized by hypertriglyceridemia and low high-density lipoprotein cholesterol), visceral obesity, and hypertension. Within the concept of MetS, the presence of hypertension plays an important role in predicting future CVD [5, 6]; however, the main determinants of hypertension within the MetS construct remain obscure. Excess caloric intake and a lack of physical activity may contribute to a state of systemic low-grade inflammation ("metaflammation") that might facilitate the development of high blood pressure [7, 8].

The adrenal cortex plays a central role in regulating blood pressure via mineralocorticoid secretion from the zona glomerulosa, acting as a key component of the renin-angiotensin-aldosterone system (RAAS). Potential adrenal alterations in MetS are an often-neglected topic, due to the scarcity of experimental models.

Our group has established a non-genomic rabbit model of MetS induced by a high-fat diet (HFD), which effectively mirrors the human MetS phenotype [9–14]. By administering an HFD for 12 weeks, we successfully induced all the hallmark features of MetS, such as hypertension, hyperglycaemia, increased visceral adiposity, and dyslipidaemia. After 12 weeks of the dietary protocol, MetS developed in approximately 70% of the HFD-fed rabbits, whereas it appeared in only 1% of those maintained on a regular diet (RD) [15]. Unlike other species, such as mice where an

HFD may elicit only some MetS components, New Zealand White rabbits reliably exhibit the full spectrum of MetS characteristics [13, 14, 16]. In addition, HFD-fed rabbits exhibited insulin resistance and dysfunctional adipose tissue [9, 10, 17]. In fact, visceral adipose tissue isolated from these animals showed insulin-resistant preadipocytes with impaired lipid metabolism, mitochondrial dysfunction, and defective adipogenesis [10]. These findings were accompanied by evidence of skeletal muscle abnormalities and a reduced propensity for physical exercise [18]. Finally, in this animal model, metaflammation was observed in all investigated tissues, including the hypothalamus, testis, epididymis, prostate, bladder, liver, and skeletal muscle [10, 12, 18]. We, therefore, hypothesized that an HFD-induced adrenal metaflammation could underlie the hypertension observed in MetS rabbits. The present study aimed to conduct a comprehensive functional, molecular, and histomorphological characterization of the adrenal glands in our established HFD rabbit model of MetS, specifically analysing steroidogenesis, metaflammation and RAAS and their correlations with the hallmarks of MetS.

Materials and methods

Animal model and ethical statement

Forty-three male New Zealand white rabbits (Charles River, Calco, Lecco, Italy), weighing about 3 kg, were individually caged under standard conditions in a temperature- and humidity-controlled room on a 12 h light/dark cycle. Water and food were unrestricted throughout the study. Experimental procedures were conducted using the facilities of the Department of Experimental and Clinical Biomedical Sciences "Mario Serio" and Department of Experimental and Clinical Medicine, and those of CE.S.A.L. (Centro Stabulazione degli Animali da Laboratorio), and NEUROFARBA Department, University of Florence, Italy.

After one-week acclimatization period on a standard diet, the animals were randomly assigned to the following groups: the control group ($n=20$) rabbits continued to receive a regular diet (RD) for 12 weeks; and the treatment group ($n=23$) rabbits were fed with a high-fat diet (HFD: RD supplemented with 0.5% cholesterol and 2.5% vegetable fat) for 12 weeks to induce metabolic syndrome (MetS), as previously described [9]. Blinding was implemented, wherever feasible, across all stages of the study, including group allocation, experimental execution, outcome assessment, and data analysis. Furthermore, the study strictly adhered to the Three Rs (Replacement, Reduction, and Refinement) principle in animal experimentation (https://www.nc3rs.org.uk/; https://awionline.org/content/the-3rs), to minimize animal utilization and avoid unnecessary sacrifice. The exact number of animals used for each specific analysis is reported in Table 1.

Rabbits were sacrificed by a lethal dose of sodium thiopental [200 mg/kg intravenous (i.v.)], and several organs, adrenals included, were harvested, weighed, and stored at -80 °C or paraffin-embedded for subsequent analyses.

All animals received human care and the animal handling complied with the Animal Welfare Body of the University of Florence, Florence, Italy, in accordance with the Italian Ministerial Law n. 26/2014. The study was approved by the Ministry of Health authorizations n. 261/2019, 146/2021 and 724/2022-PR. Animal experiments conformed to the Animal Research: Reporting of In Vivo Experiments (ARRIVE) guidelines (http://www.nc3rs.org.uk/arrive-guidelines).

Blood analysis and arterial pressure measurement

Blood samples for analyses were obtained from the marginal ear vein in both groups. All blood samples were collected in standard conditions, before 10 AM after an overnight fasting. The blood was immediately centrifuged at 2,000 *g* for 20 min at 4 °C and collected plasma/serum stored at -80 °C until assayed.

Plasma glucose, total cholesterol, and triglycerides were measured using an automated system (Cobas 8000, Roche Holding AG, Basel, Switzerland).

The oral glucose tolerance test (OGTT) was performed in accordance with the published method [9]. Briefly, after an overnight fast, a 50% glucose solution was orally administered to the animals at a dose of 1.5 g/kg. Blood samples were collected before and 15, 30, and 120 min after glucose loading. The incremental area under the curve (iAUC) was calculated by using GraphPad Prism (v. 8.4; Insight Partners, New York, NY).

Mean arterial pressure (MAP) was measured through a polyethylene arterial catheter inserted into a femoral artery at week 12, after ketamine (10 mg/kg i.v.) and sodium thiopental (50 mg/kg i.v.) sedation.

Hormone and Steroid Profile Analysis

Plasma aldosterone levels were detected by CLIA (Chemiluminescent ImmunoAssay) using the LIAISON Aldosterone assay (DiaSorin S.P.A., Saluggia, Vercelli, Italy) and an automated system (LIAISON® XL; DiaSorin S.P.A.). The analytical sensitivity of the method is characterized by a LOD of 1.45 ng/dL and a LOQ of 1.91 ng/dL. The precision of the method shows intra-assay CVs ranging between 1.8% and 4.2% and inter-assay CVs between 5.6% and 10.5%.

Other steroids have been quantified in plasma using liquid chromatography coupled with tandem mass spectrometry

Table 1 Sample size summary table

Analysis & Methodology	Samples size (n)	
Systemic & Metabolic Profiling	**RD**	**HFD**
Metabolic & hemodynamic assessment[1]	20	23
Histological & Tissue Analysis	**RD**	**HFD**
Adrenal morphometric analysis	3	3
Tissue inflammation (Giemsa)	5	6
Macrophage infiltration (RAM11 IHC/IF)	5	7
Fibrosis quantification (PSR)	5	7
Adrenal steroidogenesis (CYP21A2 IHC)	6	6
Gene Expression (RT-qPCR)	**RD**	**HFD**
Pro-inflammatory markers[2]	7	9
RAAS components[3]	20	23
CRH in hypothalamus	12	12
Steroidogenesis enzymes[4]	8	10

[1]Includes blood analysis, Oral Glucose Tolerance Test (OGTT), Mean Arterial Pressure (MAP), and steroid profiling. [2]*CD68*, *CD11c*, and *TBX21*. [3]Angiotensinogen, renin, angiotensin-converting enzyme 2, and angiotensin receptor 1. [4]*STAR*, *CYP11A1*, *CYP11B1* and *CYP11B2* (aldosterone synthase)

Abbreviations: IHC, Immunohistochemistry; IF, Immunofluorescence; PSR, Picrosirius Red; RAAS, Renin-Angiotensin-Aldosterone System *CRH*, Corticotropin-Releasing Hormone

(LC-MS/MS) using a Sciex 6500QTRAP instrument (Sciex, Framingham, MA) equipped with a 1260 HPLC (Agilent Technologies, Santa Clara, CA). Briefly, to precipitate the proteins, 200 µL of plasma were added to 400 µL of acetonitrile containing the internal standards at the following concentrations: P, progesterone 2,3,4-$^{13}C_3$ (1.25 ng/mL, Sigma-Aldrich); B, corticosterone-$^{13}C_3$ (5 ng/mL, Cerilliant, Round Rock, TX) 17-OH-P, 17-hydroxyprogesterone 2,3,4-$^{13}C_3$ (0.0625 ng/mL, Sigma-Aldrich); F, cortisol 9,11,12,12-D_4 (6.25 ng/mL, CDN isotopes, Pointe-Claire, Canada); E, cortisone 1,2-D_2 (0.4 ng/mL, CDN Isotopes); B, corticosterone-$^{13}C_3$ (5 ng/mL, Cerilliant, Round Rock, TX);. Corticosterone was used as internal standard for 11-deoxycorticosterone (11-DOC), whereas cortisol was used as internal standard for 11-deoxycortisol.

To quantify the samples, Mass Chrom Multilevel serum calibrator set Panel I&II (Chromosystems Instruments & Chemicals GmbH, Gräfelfing, Germany) was used, with the following reported concentrations: P (0.43–79.50 nM); B (1.53–132 nM); 11-deoxycorticosterone (0.133–8.81 nM); 17-OH-P (0.26–43.90 nM); F (27.6–770.0 nM); 11-deoxycortisol (0.26–39.50 nM); B (1.53–132 nM); 11-deoxycorticosterone (0.133–8.81 nM).

Samples were centrifuged for 10 min at 8000 *g*, and the supernatant was transferred into a clean vial. Then, 500 µL of water was added, and 25 µL were injected into the LC-MS/MS system.

Separation was achieved using an online SPE configuration, consisting of a washing/pre-concentrating C18 column (5 µm, 20 × 2 mm) and an analytical column - a Kinetex XB-C18 (2.6 µm, 100 × 3 mm). All HPLC columns were obtained from Phenomenex (Torrance, CA). Samples were loaded onto the SPE column and flushed with a water: methanol mixture (95:5, v/v) using an isocratic system. Analytical separation was then performed using a gradient composed of water with ammonium fluoride and methanol. The mass spectrometer operated in Multiple Reaction Monitoring (MRM) in positive ion modes. Quantitation was done using MULTIQUANT software (Sciex).

Histological staining

Adrenal glands were fixed in 10% buffered formalin (Sigma-Aldrich Corp., St. Louis, MO), paraffin embedded and sectioned at a thickness of 5 µm with a microtome. For general morphological assessment, tissue sections were stained with hematoxylin and eosin (H&E; both Bio-Optica, Milan, Italy), according to standard protocols routinely adopted for histological evaluation. Morphometric analysis was performed on whole-slide images acquired using an Ocus 40 digital microscope (Grundium, Tampere, Finland). To further characterize inflammatory infiltration and lipid accumulation, adrenal gland sections were subjected to Giemsa and Masson's trichrome staining, respectively. Briefly, after deparaffinization and graded rehydration, slides were incubated

with Giemsa solution (Bio-Optica) diluted in distilled water at ratio 1:1, or processed with Masson's trichrome kit (Bio-Optica), following the manufacturer's instructions, as previously detailed in similar experimental settings [11].

Giemsa staining was used as a complementary histological approach to visualize inflammatory foci in adrenal tissue [19] and to obtain a descriptive semi-quantitative estimate of inflammatory status. Inflammatory foci were scored using an adapted scheme from Kleiner et al. [20] based on the number of foci per 200x field: 0, absence of inflammatory foci; 1, fewer than two foci; 2, two to four foci; and 3, more than four foci. This scoring approach was originally developed and validated for liver histopathology, and applied here as a general descriptive semi-quantitative metric for adrenal gland inflammatory status.

Collagen content was evaluated and quantified using Picrosirius Red Stain kit (Bio-Optica), as per manufacturer's instructions. Briefly, deparaffinized and rehydrated sections were incubated with the staining solution for 50 min, rinsed with the appropriate reagents and distilled water, dehydrated through ascending alcohols and xylene, and subsequently mounted, as previously described [21]. Semi-quantitative analysis of Picrosirius Red-positive areas was performed by measuring the percentage of the stained area in at least four 100X fields per slide using ImageJ software (https://imagej.net/). All histological sections were evaluated in a blinded manner and imaged using a Nikon Microphot-FXA light microscope (Nikon, Tokyo, Japan). For each animal, measurements from six analysed slices were averaged to obtain a single quantitative value. Overview images for Giemsa and H&E stainings were obtained by digitally merging adjacent microscopic fields using the Photomerge function in Adobe Photoshop software (Adobe Systems Inc., San Jose, CA, USA).

Immunohistochemistry and immunofluorescence

Immunohistochemistry was performed to analyse the presence of macrophages and CYP21A2 expression in adrenal gland. Briefly, paraffin embedded adrenal sections (5µm) were deparaffinized, rehydrated and, after antigen retrieval, incubated overnight at 4°C with mouse monoclonal anti-RAM11 (rabbit macrophage marker; 1:80; MO633; Dako, Carpenteria, CA) or mouse monoclonal anti-CYP21A2 (1:100; Abcam, Cambridge, UK; 1:800; Santa Cruz Biotechnology, Dallas, TX) antibody, followed by biotinylated anti-mouse secondary antibody (Millipore, Burlington, MA) and streptavidin-peroxidase complex (Millipore). The reaction product was developed with 3',3'-diaminobenzidine tetrahydrochloride as chromogen (Merck KgaA, Darmstadt, Germany). Negative controls were performed by avoiding the primary antibody. Densitometric analysis of CYP21A2 immunostaining was performed by measuring the percentage of the stained area within the zona fasciculata using ImageJ software (https://imagej.net/). For each animal, measurements from six analysed slices were averaged to obtain a single quantitative value.

The expression of the macrophages was further investigated by immunofluorescence analysis. Briefly, paraffin-embedded adrenal Sect. (5 µm) were deparaffinized and rehydrated, followed by heat-induced antigen retrieval in 10 mM sodium citrate buffer (pH 6.0; Zitomed System, Berlin, Germany). After blocking in PBS containing 1% bovine serum albumin for 45 min at room temperature, sections were incubated overnight at 4 °C with mouse monoclonal anti-RAM11 antibody (1:100; Dako). Immunofluorescent detection was performed using Alexa Fluor 568-conjugated donkey anti-mouse IgG secondary antibody (1:200; Thermo Fisher Scientific, Waltham, MA, USA), incubated in the dark. Negative controls were obtained by omitting the primary antibody. All slides were evaluated blindly and photographed using a Nikon Microphot-FXA microscope (Nikon).

Gene expression analysis

TRIzol reagent (Life Technologies, Paisley, UK) and RNeasy Mini Kit (Qiagen, Hilden, Germany) were used to isolate total RNA from rabbit adrenal, hypothalamus, liver, kidney and lung specimens. cDNA synthesis was carried out using the iScriptTM cDNA Synthesis Kit (Bio-Rad Laboratories, Hercules, CA). Semi-quantitative real-time RT-PCR (qRT-PCR) amplification and detection was performed with SsoAdvancedTM Universal SYBR® Supermix and a CFX96 Duet Real-Time PCR Detection System (both Bio-Rad Laboratories). Specific PCR primers for rabbit target genes were designed on sequences available at the National Center for Biotechnology Information GenBank (http://www.ncbi.nlm.nih.gov) or Ensemble Genome (http://www.ensembl.org). The 18 S ribosomal RNA subunit was used as the housekeeping gene for the relative quantitation of the target genes based on the comparative threshold cycle (Ct) 2-ΔΔCt method [22], with some modifications. In detail, we used the control group as the calibrator in each analysis, so that the calculations would provide the fold-change of the other group relative to control.

Statistical analysis

Statistical analysis was performed using SPSS version 29.0 (IBM Corporation). Data visualization and graphical representation were generating using GraphPad Prism Version 10 (GraphPad Software). The distribution of data was assessed using the Shapiro-Wilk test. Normally distributed data were

compared using an unpaired Student's t-test and are presented as mean ± standard deviation (SD). Non-normally distributed data were compared using the Mann-Whitney U test and are presented as median [minimum - maximum]. P-values obtained from the individual comparisons were adjusted for multiple testing across all variables analysed within the same experimental comparison using the Benjamini-Hochberg false discovery rate procedure. Statistical significance was defined as a BH-adjusted p-value < 0.05. Associations between categorical variables were analysed using contingency tables, and statistical significance has been evaluated using the Monte Carlo method implemented in SPSS (10,000 random samples). Correlations between variables were assessed using Spearman's rank correlation coefficient. A p-value of < 0.05 was considered statistically significant.

Results

High fat diet induces profound adrenal histomorphological changes

In the present rabbit model of metabolic syndrome, we observed distinct morphological differences in the adrenal glands. Rabbits fed an HFD exhibited a steatotic appearance and texture, together with a significant increase in both the absolute size and weight of the adrenal glands compared to those on a regular diet (RD) (adrenal weight: RD = 0.605 [0.44–1.26] g vs. HFD = 1.350 [1.04–2.11] g; $p < 0.001$, data not shown). This increase was also significant when normalized to the animal's body weight (Adrenal weight% of total: RD = 0.016% [0.011–0.033] vs. HFD = 0.040% [0.027–0.066]; $p < 0.001$, Fig. 1b).

Accordingly, morphometric analysis of adrenal sections indicated an increase in overall cortical thickness in HFD rabbits ($n = 3$) relative to RD animals ($n = 3$). Specifically, total cortical thickness was increased in the HFD group (RD = 2754 ± 1815 µm vs. HFD = 6176 ± 157 µm), reflecting an expansion of the combined zona fasciculata and zona reticularis (RD = 2492 ± 1757 µm vs. HFD = 5896 ± 308 µm), whereas the thickness of the zona glomerulosa remained comparable between groups (RD = 232 ± 81 µm vs. HFD = 280 ± 182 µm). Although these differences did not reach statistical significance — likely due to the limited sample size and marked inter-individual variability in the RD group — the morphometric trend consistently pointed to cortical enlargement in HFD animals.

At the histological level, haematoxylin and eosin (H&E) staining (Fig. 1c) revealed increased vacuolization and clear areas in the adrenal cortex of HFD rabbits, indicative of structural alterations consistent with high lipid content. In line with the H&E findings, Masson's trichrome staining (Fig. 1d) showed marked remodelling of the cortical architecture, with stromal components delineating areas characterized by vacuolar changes in HFD adrenal glands.

Given the known link between MetS and inflammation, we evaluated adrenal tissue inflammation using Giemsa

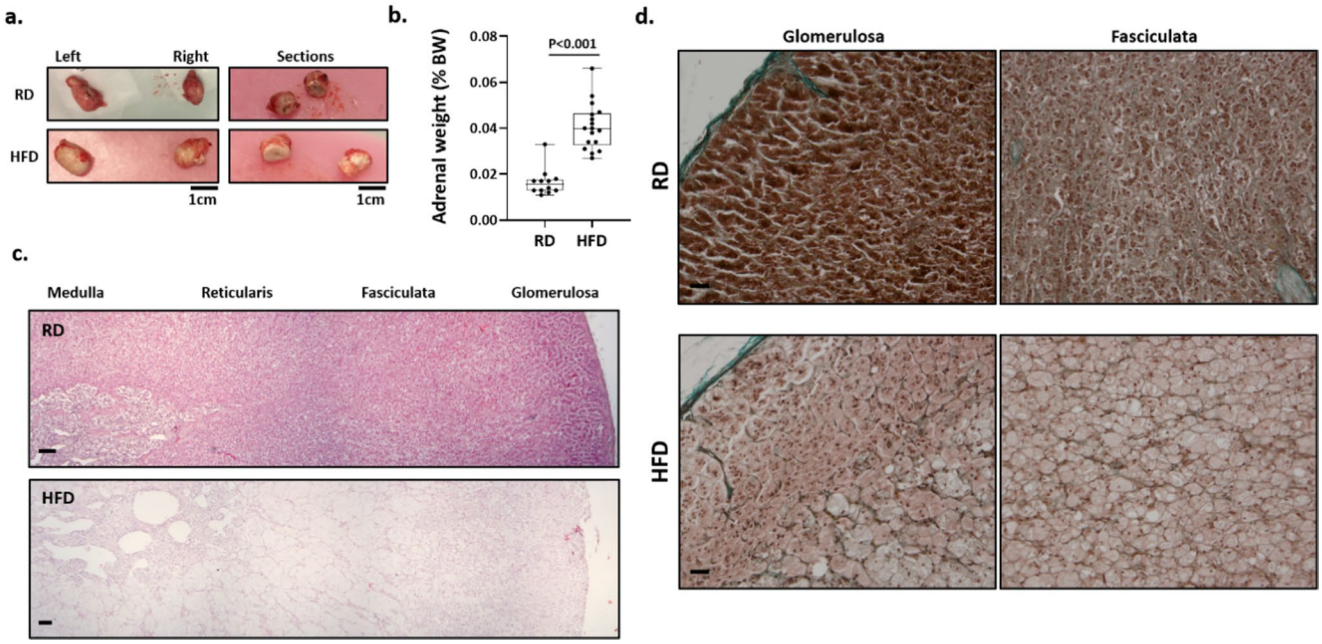

Fig. 1 Adrenal gland morphology and weight in RD and HFD rabbits. **a**: Representative images of intact adrenal glands and sections. **b**: Comparison of total adrenal weight (expressed as % of total body weight) between the two groups. **c**: Representative H&E and **d**: Masson's trichrome-stained adrenal sections, with histological zones indicated. Scale bars = 100 µm

staining (Fig. 2). Figure 2a-b shows representative cross-sections of adrenal tissue from RD and HFD rabbits, providing an overview of tissue morphology. As shown in Fig. 2c, quantitative analysis of Giemsa-stained sections, based on the quantification of inflammatory foci, demonstrated a significantly increased inflammation score in the HFD group compared with RD animals ($p=0.048$).

To further characterize adrenal inflammation, immunohistochemical and immunofluorescence analyses were performed using RAM11, a validated rabbit macrophage marker [23] recognizing connective tissue and vascular-associated macrophages. Immunohistochemical analysis revealed intense RAM11 immunoreactivity in adrenal glands from HFD rabbits compared with RD animals, indicating increased macrophage infiltration (Fig. 3a). This finding was further supported by immunofluorescence analysis, which provided a more detailed visualization of macrophage distribution and showed a prominent accumulation of RAM11-positive cells, primarily in the zona fasciculata and particularly at the interface with the zona glomerulosa (Fig. 3b).

We also evaluated the mRNA expression levels of CD68, CD11c, and TBX21, which serve as markers for different types of immune cells involved in inflammatory responses. Specifically, CD68 is a marker for monocytes and macrophages; CD11c is expressed on macrophages, monocytes, and certain lymphocytes; and TBX21 is a master regulator of Th1 cells. Interestingly, the adrenal tissue of HFD rabbits showed significantly higher mRNA expression of CD68 (230 ± 131% of RD; $p=0.044$), CD11c (3287 ± 1773% of RD; $p=0.005$), and TBX21 (284 ± 167% of RD; $p=0.026$) (Fig. 3c), indicating a shift toward a pro-inflammatory phenotype.

Quantitative analysis of Picrosirius Red staining, which selectively identifies collagen fibers, demonstrated a significant increase in fibrosis within the zona fasciculata of the HFD group compared to the RD group. The median percentage of the fibrotic area was significantly higher in the HFD group compared to the RD group (RD: 0.044% [0.021–0.058] vs. HFD: 3.93% [1.72–5.33]; $p=0.002$; Fig. 3d).

High fat diet alters the hormone and steroid profile

As expected in this MetS model, HFD animals were hypertensive (mean arterial pressure: HFD = 139.60 ± 27.56 mmHg vs. RD = 85.54 ± 17.87 mmHg; $p<0.001$; Fig. 4a). Given this finding and the aforementioned adrenal alterations, we investigated adrenal function by measuring circulating aldosterone levels. Intriguingly, aldosterone levels were significantly lower in HFD rabbits compared to RD (HFD = 17.5 [4.5–166.5] ng/dL vs. RD = 59 [16–134] ng/dL; $p=0.044$; Fig. 4a). To explore potential underlying mechanisms, we analysed the components of the renin-angiotensin system (RAAS) in various tissue homogenates. HFD animals

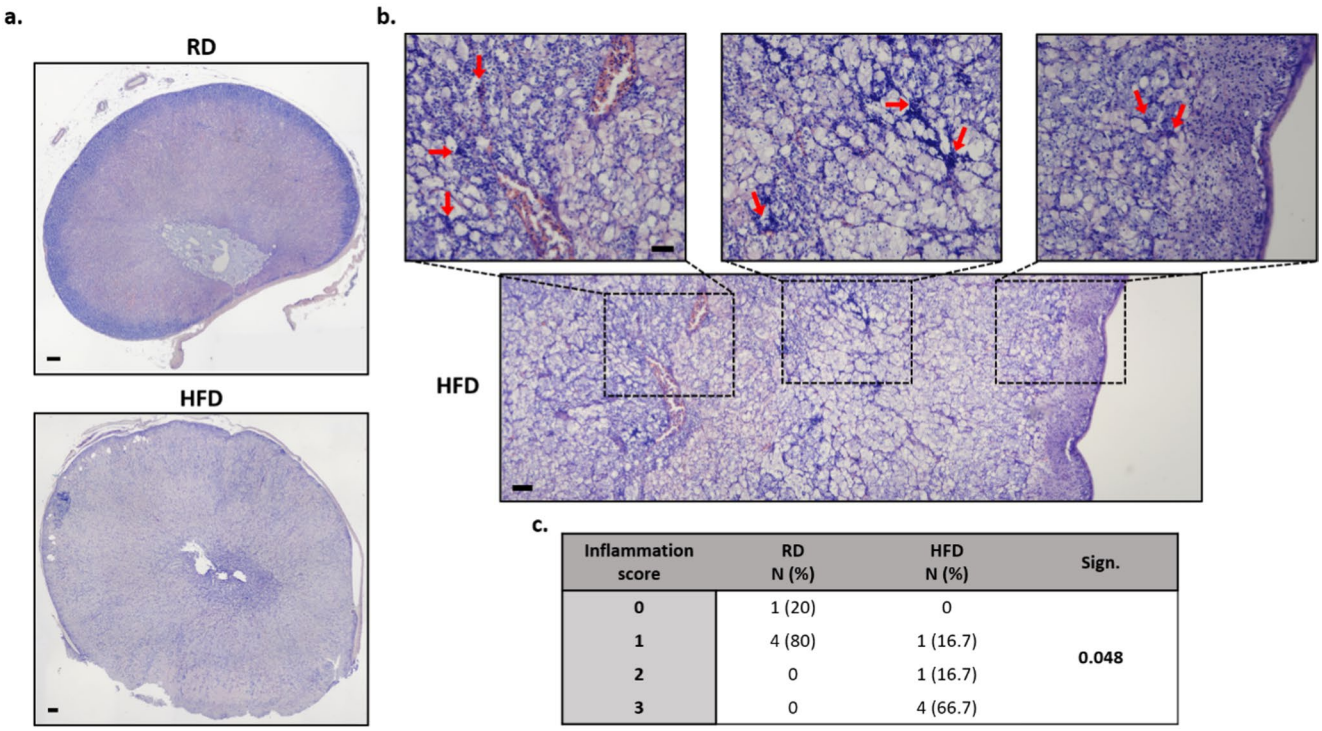

Inflammation score	RD N (%)	HFD N (%)	Sign.
0	1 (20)	0	0.048
1	4 (80)	1 (16.7)	
2	0	1 (16.7)	
3	0	4 (66.7)	

Fig. 2 Adrenal gland inflammation assessment in RD and HFD rabbits. **a**, **b**: Representative Giemsa-stained adrenal sections at **(a)** low magnification (scale bar = 200 µm) and **(b)** high magnification in HFD rabbits (scale bar = 100 µm), where red arrows indicate inflammatory foci. **c**: Contingency table comparing inflammation scores between the RD and HFD groups ($n=5$ for RD, $n=6$ for HFD)

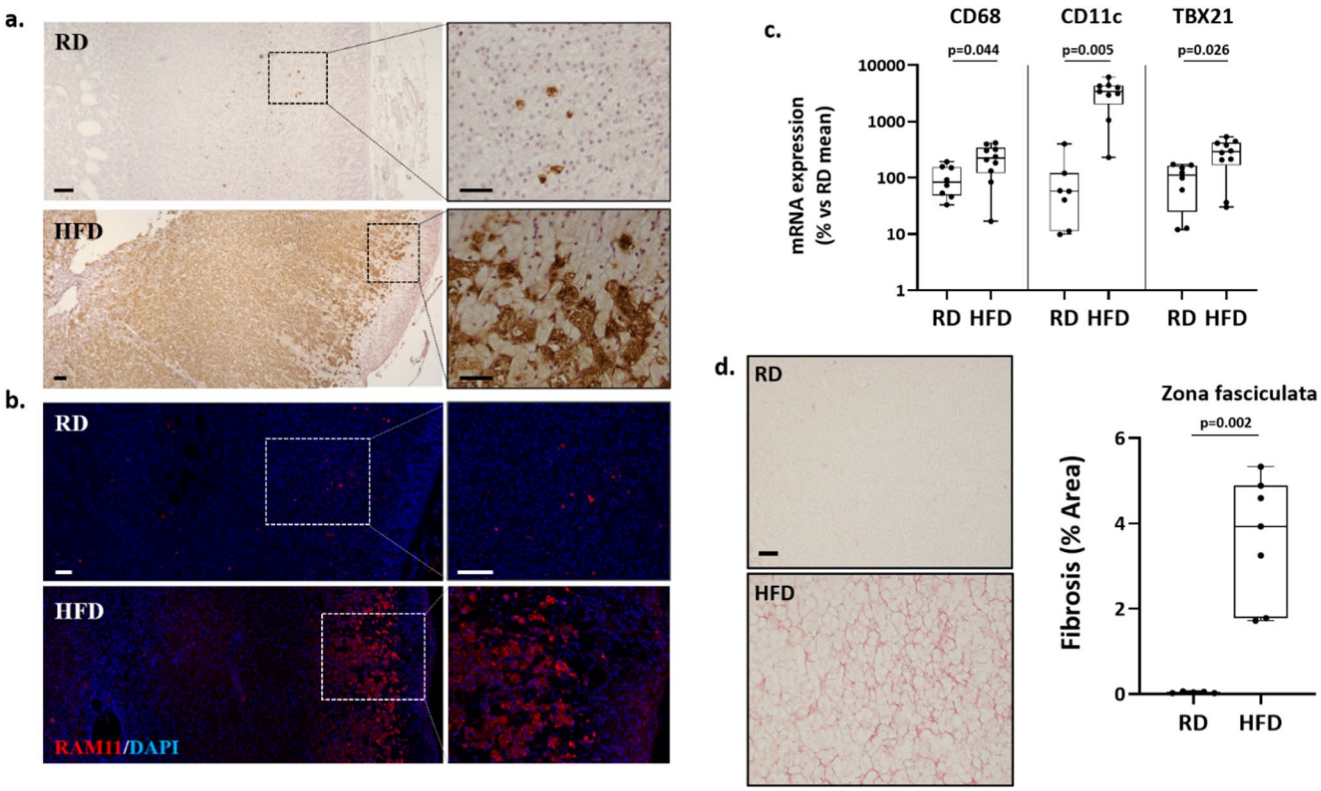

Fig. 3 Macrophage infiltration, gene expression, and fibrosis in adrenal glands of RD and HFD rabbits. **a**, **b**, **d**: Representative images of (**a**) RAM11 immunohistochemistry, (**b**) RAM11 immunofluorescence, and (**d**) Picrosirius red (PSR) staining. Scale bars: 100 µm. (**c**) Relative gene expression of pro-inflammatory markers (CD68, CD11c, TBX21), reported as percentage of the RD mean. Sample sizes (n) for RD and HFD, respectively: (**a**, **b**, **d**) 5, 7; (**c**) 7, 9. PSR quantification is expressed as percentage of fibrotic area

exhibited a statistically significant reduction in the mRNA expression of: renin (REN) in the kidneys (31.59 ± 54.5% of RD; $p = 0.003$); angiotensin-converting enzyme 2 (ACE2) in the lungs (51.93% ± 39.2% of RD; $p = 0.003$); and angiotensin receptor 1 (AGTR1) in the adrenals (51.92% ± 17.19% of RD; $p = 0.01$) (Fig. 4b). Angiotensinogen (AGT) in the liver, instead, exhibited a non-significant downward trend (77.13 ± 33.76% of RD; $p = 0.141$).

We also assessed adrenal steroidogenesis, revealing lower expression of STAR (33.03 ± 11.89% of RD; $p = 0.003$), CYP11A1 (32.42 ± 16.39% of RD; $p = 0.026$), and CYP11B2 (39.16% ± 21.27% of RD; $p = 0.009$), with no significant differences in CYP11B1 expression (63.96% ± 61.41% of RD; $p = 0.373$, Fig. 4c). The analysis moreover showed a reduction, though non statistically significant, of melanocortin 2 receptor (MC2R, 61.46 ± 27.65% of RD; $p = 0.06$). Consistent with the CYP11B2 decrease, circulating levels of the upstream steroids 11-deoxycorticosterone (11-DOC) (HFD = 10.49 [2.66–126.23] nM vs. RD = 3.16 [0.49–23.72] nM; $p < 0.001$) and progesterone (HFD = 2.40 [1.00–7.60] nM vs. RD = 0.82 [0.36–10.71] nM; $p = 0.002$) were significantly elevated in the HFD group. No differences were observed in corticosterone levels (HFD = 98.75 [14.27–290.22] nM vs. RD = 132.70 [15.41–440.28] nM; $p = 0.898$) (Fig. 4d) and hypothalamic CRH mRNA expression (122.18 ± 77.04% of RD; $p = 0.260$).

No significant differences were observed in the levels of 11-deoxycortisol (HFD = 14.15 ± 9.0 nM vs. RD = 20.59 ± 12.7 nM; $p = 0.326$), cortisol (HFD = 17.09 [1.07–62.05] nM vs. RD = 12.24 [1.68–31.88] nM; $p = 0.348$), or cortisone (HFD = 1.77 [1.10–5.53] nM vs. RD = 1.70 [1.32–4.64] nM; $p = 0.935$).

Furthermore, immunohistochemical staining for CYP21A2, demonstrated higher overall expression of the enzyme in the HFD group compared to the RD group (HFD = 15.91% ± 7.38% vs. RD = 4.06% ± 2.26%, $p = 0.004$; Fig. 5), exhibiting a patchy expression in the fasciculata and reticularis, with an almost absent staining in the glomerulosa.

Finally, 11-DOC levels showed significant positive correlations with all primary MetS features (Table 2). Furthermore, 11-DOC concentrations were negatively correlated with aldosterone levels (rho = -0.381; $p = 0.05$), underscoring a severely dysregulated steroidogenic pathway.

Furthermore, similar positive correlations have been found between P and all primary MetS features as well as between 11-DOC and P, further emphasizing the

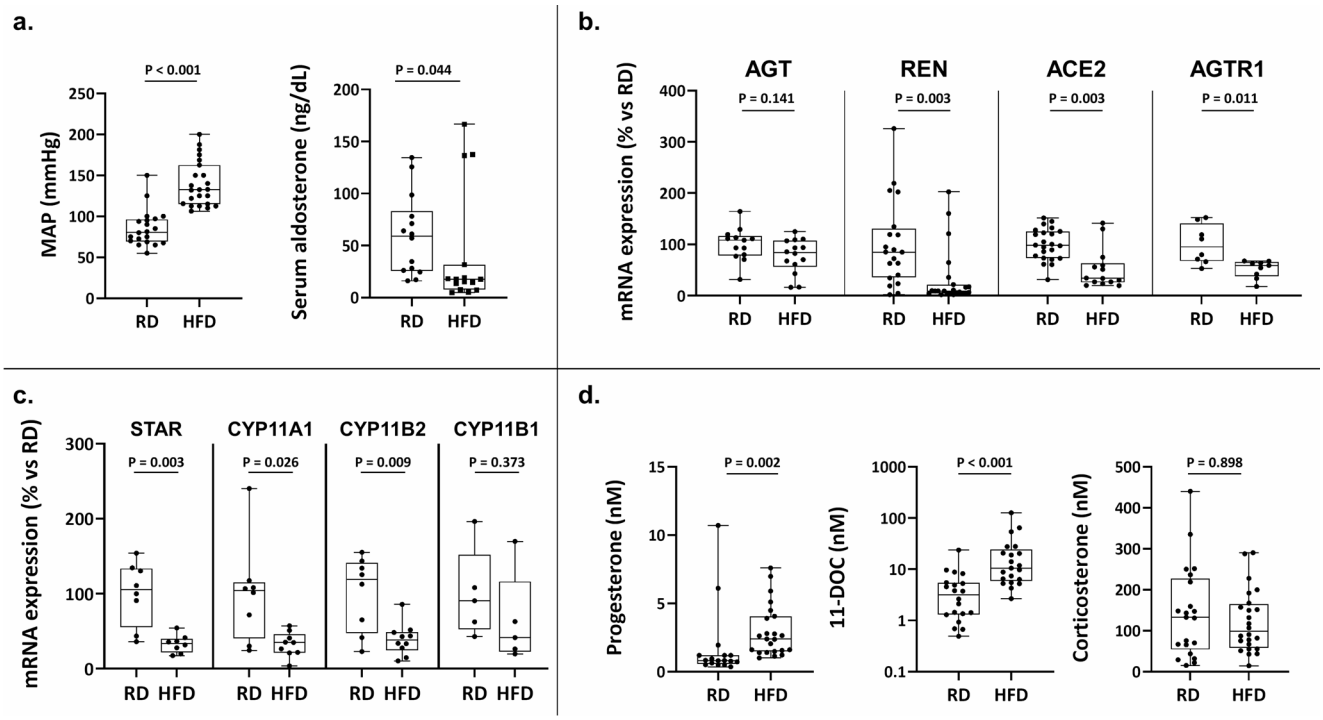

Fig. 4 Arterial pressure, the renin-angiotensin system, steroids, and steroidogenic enzymes in RD and HFD groups. **a**: Mean arterial pressure and aldosterone concentrations. **b**: Tissue-specific gene expression of renin-angiotensin system components: *AGT* (angiotensinogen in liver), *REN* (renin in kidney), *ACE2* (angiotensin-converting enzyme 2 in lung), and *AGTR1* (angiotensin receptor 1 in adrenal). **c**: Adrenal gene expression of glucocorticoid synthesis pathway enzymes: *STAR*, *CYP11A1* (Cholesterol side chain cleavage enzyme), *CYP11B1* (11-hydroxylase), and *CYP11B2* (aldosterone synthase). **d**: Peripheral blood concentrations of steroid precursors: progesterone, 11-deoxycorticosterone (11-DOC), and corticosterone. Sample sizes (n) for RD and HFD, respectively: (**a**, **b**, **d**) 20, 23; (**c**) 8, 10

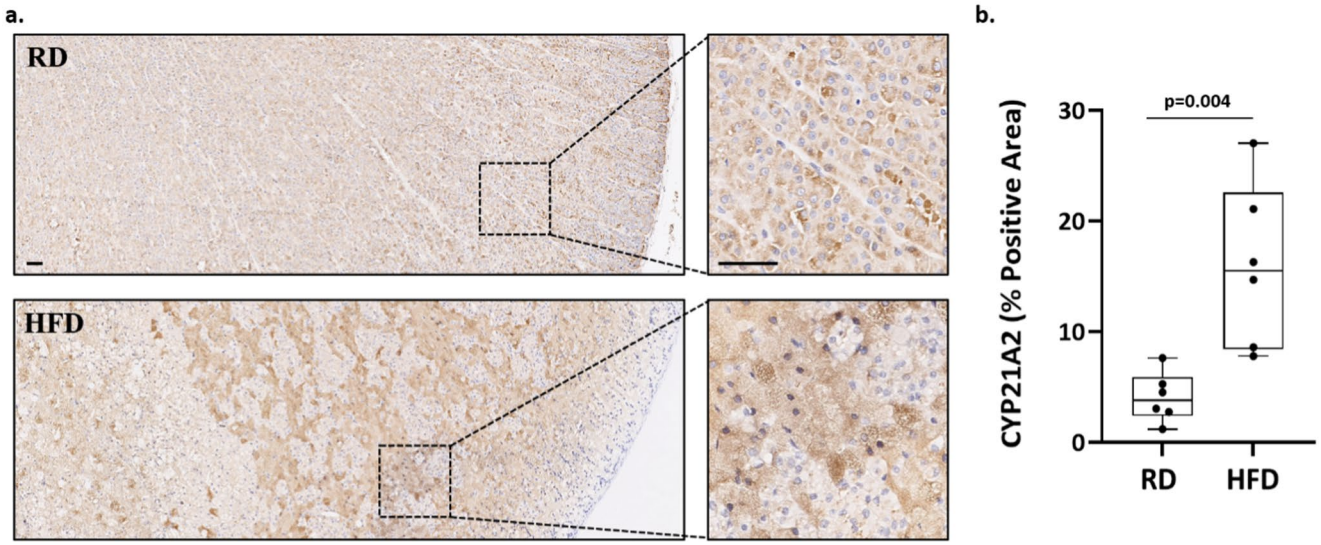

Fig. 5 Adrenal gland CYP21A2 expression in RD and HFD rabbits. **a** Representative CYP21A2 immunohistochemistry images of adrenal sections from both experimental groups. **b** Quantitative CYP21A2 expression. Sample sizes: $n = 6$ per group. Scale bars = 50 µm

Table 2 Correlations between steroids levels and metabolic and biochemical parameters of Mets

	11-DOC (nM)	Glycemia (gr/L)	OGTT (iAUC)	Triglycerides (mg/dL)	MAP (mmHg)	VAT (%BW)
11-DOC (nM)		ρ = 0.548 **p < 0.001**	ρ = 0.582 **p < 0.001**	ρ = 0.507 **p < 0.001**	ρ = 0.560 **p < 0.001**	ρ = 0.598 **p < 0.001**
Corticosterone (nM)	ρ = 0.529 **p < 0.001**	ρ = 0.055 p = 0.719	ρ = 0.077 p = 0.616	ρ = -0.114 p = 0.455	ρ = 0.040 p = 0.810	ρ = 0.180 p = 0.237
Aldosterone (ng/dL)	ρ = -0.381 **p = 0.050**	ρ = -0.387 **p = 0.038**	ρ = -0.448 **p = 0.015**	ρ = -0.397 **p = 0.033**	ρ = -0.349 p = 0.103	ρ = -0.299 p = 0.115
Progesterone (nM)	ρ = 0.718 **p < 0.001**	ρ = 0.555 **p < 0.001**	ρ = 0.645 **p < 0.001**	ρ = 0.587 **p < 0.001**	ρ = 0.534 **p < 0.001**	ρ = 0.393 **p = 0.012**
11-Deoxycortisol (nM)	ρ = 0.135 p = 0.581	ρ = -0.163 p = 0.492	ρ = -0.203 p = 0.391	ρ = -0.457 **p = 0.043**	ρ = -0.251 p = 0.331	ρ = -0.023 p = 0.925
Cortisol (nM)	ρ = 0.232 p = 0.155	ρ = 0.136 p = 0.391	ρ = 0.103 p = 0.518	ρ = 0.073 p = 0.648	ρ = 0.115 p = 0.504	ρ = 0.364 **p = 0.018**
Cortisone (nM)	ρ = -0.157 p = 0.496	ρ = -0.146 p = 0.507	ρ = -0.106 p = 0.563	ρ = -0.079 p = 0.720	ρ = -0.065 p = 0.798	ρ = 0.132 p = 0.547

Abbreviations: 11-DOC, 11-deoxycorticosterone; OGTT (iAUC) = oral glucose tolerance test (incremental area under curve); MAP, mean arterial pressure; VAT, visceral adipose tissue; BW, Body Weight

steroidogenetic disarray with accumulation of metabolites in the mineralocorticoid pathway.

In contrast, corticosterone, and cortisone did not show any significant association with MetS features. 11-Deoxycortisol and cortisol showed isolated significant correlations, respectively with triglycerides (rho = -0.457; $p = 0.043$) and visceral adipose tissue (rho = 0.364; $p = 0.018$).

Discussion

In this study, we investigated the involvement of the adrenal cortex in the pathophysiology of hypertension within the metabolic syndrome paradigm, using a rabbit model. Our findings demonstrate that chronic exposure to a high-fat diet induces adrenal steatotic metaflammation, associated with distinct morphological modifications and steroidogenic alteration. We hypothesize that these alterations promote a 11-DOC driven hypertension, occurring with a concomitant downregulation of the RAAS.

It is well established that chronic exposure to a high-fat diet leads to metabolic dysfunction characterized by steatosis, inflammation, and fibrosis in multiple organs [1, 10–12]. In the liver, the associated lipid accumulation, fibrosis, and inflammatory infiltration triggers the development of metabolic dysfunction-associated steatotic liver disease (MASLD) [24]. Our findings suggest that a similar process may occur in the adrenal cortex. We have termed this clinical-pathological entity Metabolic Dysfunction-Associated Steatotic Adrenal Disease (MASAD).

The MASAD phenotype in our model is characterized by significant hypertrophy of the adrenal cortex, driven by intracellular lipid accumulation especially in the zona fasciculata, where an extensive vacuolar pattern and the disruption of normal cortical organization were observed. This lipid overload may trigger a robust inflammatory response, as evidenced by macrophage infiltration, the upregulation of pro-inflammatory markers, and the development of fibrosis. These processes may subsequently lead to disruption of the normal zonation of the adrenal cortex, potentially leading to steroidogenic alterations.

Concurrent with the presence of arterial hypertension, HFD rabbits showed low levels of aldosterone, accompanied by systemic suppression of the entire Renin-Angiotensin-Aldosterone System (RAAS). We propose that hypertension, in this context, could be driven by the accumulation of steroid precursors, especially 11-DOC, as a consequence of *CYP11B2* downregulation. The negative correlation between 11-DOC and aldosterone levels, moreover, further suggests a negative feedback mechanism where precursor accumulation suppresses aldosterone synthesis. The concomitant increase in progesterone, a direct precursor of 11-DOC, may further amplify this effect through MR sensitization [25]. The significant correlations between 11-DOC, progesterone and all MetS hallmarks underscore the strong relationship between metabolic alterations and steroidogenic disarray.

In addition, possibly contributing to the 11-DOC accumulation, we identified an increase of *CYP21A2* expression, accompanied by disruption of the normal distribution of this enzyme, predominantly localized to the zona fasciculata and reticularis and almost absent in the glomerulosa, leading to a "patchy" and disorganized pattern. We hypothesize that inflammation and fibrosis may lead to the isolation of cell clusters, disrupting the normal organization of the adrenal cortex and altering the expression and coordination of steroidogenic enzymes.

As 11-DOC possesses mineralocorticoid activity [26], its accumulation may provide a link between adrenal

lipotoxicity and hypertension. Markedly elevated 11-DOC levels may, through MR activation, promote sodium retention, suppressing renin secretion through increased renal perfusion pressure and sodium delivery to the macula densa, resulting in a low-renin and low-aldosterone hypertension model. This 11-DOC-driven hypertension is similar to that observed in 11β-hydroxylase deficiency (11β-OHD), where loss-of-function mutations in the *CYP11B1* gene [27] prevents the conversion of 11-deoxycortisol to cortisol and 11-DOC to corticosterone in the zona fasciculata, reducing feedback inhibition on the hypothalamus and anterior pituitary. The subsequent increase in ACTH secretion chronically stimulates the zona fasciculata, ultimately leading to the accumulation of precursor steroids, particularly 11-DOC, suppressing the RAAS and leading to low-renin hypertension and potential hypokalemia [28, 29].

Interestingly, despite a non-significant downward trend in adrenal *MC2R* expression, accompanied by a corresponding, non-significant reduction in its downstream target *CYP11B1*, there was not a significant change in circulating cortisol or corticosterone levels. This suggests that, despite a possible mild impairment of ACTH receptor signaling, the glucocorticoid axis remains largely preserved in this model, as similarly reported by Toth et al. on the same animal model [30]. Finding of unchanged level of CRH in the media preoptic area of the hypothalamus between groups further suggest no major alteration in the glucocorticoid axis.

Our study confirms that a high-fat diet (HFD) induces histopathological alterations in the adrenal gland, as previously described in a similar rabbit model [31]. However, our functional findings appear to conflict with those of Swierczynska et al., who observed in an HFD-fed mice model, adrenal hyperplasia and functional activation of steroidogenesis with increased expression of *STAR*, *CYP11A1*, *CYP21A2*, and *CYP11B1*, along with elevated levels of progesterone, corticosterone, and aldosterone [32]. Our rabbit model instead, reveals altered steroidogenesis characterized by a downregulation of the aldosterone synthase pathway and the accumulation of biologically active precursors. This difference might be due to interspecies variability in adrenal steroidogenesis and response to high-fat diets.

This study has some limitations: we were unable to provide data on rabbit treated chronically with MR antagonist, such as spironolactone, that could be the proof of concept of the present study. We did not observe significant hypokalemia in the HFD rabbits, most probably because the serum was always hyperlipemic and often haemolyzed. Hence, results on electrolyte measurements were not reliable. Some experiments have been performed on limited samples, therefore reducing the generalizability of the results. Other limitations are the lack of determinations of circulating ACTH and renin due to technical reasons, and therefore the use of surrogate markers of the same as respectively, hypothalamic CRH and kidney renin mRNA expression. Finally, no a priori power calculation was performed; sample sizes were instead determined based on the 3Rs principle and on previous studies using this animal model.

To our knowledge, this is the first study to link HFD-induced adrenal lipid accumulation, macrophage infiltration, inflammation, and fibrosis to a specific steroidogenic alteration in a rabbit model. While the classical phenotype in human metabolic syndrome is often associated with high RAAS activity, our model suggests that in cases of severe adrenal lipotoxicity, the hormonal profile may shift, as shown in the graphical abstract.

In conclusion, our data support the hypothesis that the HFD-induced adrenal metaflammation may disrupt the normal steroidogenic flux leading to an accumulation of mineralocorticoid precursors independently of RAAS activation. This would identify the adrenal gland not merely as a target of metabolic insult, but as an active endocrine driver of a paradoxical 'low-renin, low-aldosterone' hypertension in the context of metabolic syndrome, via a non-canonical, 11-DOC-mediated MR activation.

Funding Open access funding provided by Università degli Studi di Firenze within the CRUI-CARE Agreement. This research was supported by the Italian Association for Cancer Research (AIRC, under IG 2020-ID 24820 project for Mario Maggi).

Declarations

Conflict of interest The authors declare that the research was conducted in the absence of financial or non-financial that are relevant to the content of this article.

Ethics approval The study was approved by the Ministry of Health authorizations n. 261/2019, 146/2021 and 724/2022-PR.

References

1. Hotamisligil GS (2006) Inflammation and metabolic disorders. Nature 444(7121):860–867. https://doi.org/10.1038/nature05485
2. Shoelson SE (2006) Inflammation and insulin resistance. J Clin Invest 116(7):1793–1801. https://doi.org/10.1172/JCI29069

3. Calder PC (2017) Omega-3 fatty acids and inflammatory processes: from molecules to man. Biochem Soc Trans 45(5):1105–1115. https://doi.org/10.1042/BST20160474
4. Zhou B, Rayner AW, Gregg EW et al (2024) Worldwide trends in diabetes prevalence and treatment from 1990 to 2022: a pooled analysis of 1108 population-representative studies with 141 million participants. Lancet 404(10467):2077–2093. https://doi.org/10.1016/S0140-6736(24)02317-1
5. Liu J, Chen Y, Cai K, Gong Y (2021) Association of metabolic syndrome with cardiovascular outcomes in hypertensive patients: a systematic review and meta-analysis. J Endocrinol Invest 44(11):2333–2340. https://doi.org/10.1007/s40618-021-01603-7
6. Ndumele CE, Neeland IJ, Tuttle KR et al (2023) A Synopsis of the Evidence for the Science and Clinical Management of Cardiovascular-Kidney-Metabolic (CKM) Syndrome: A Scientific Statement From the American Heart Association. Circulation 148(20):1636–1664. https://doi.org/10.1161/CIR.0000000000001186
7. Silveira Rossi JL, Barbalho SM, Reverete De Araujo R, Bechara MD, Sloan KP, Sloan LA (2022) Metabolic syndrome and cardiovascular diseases: Going beyond traditional risk factors. Diabetes Metab Res Rev 38(3):e3502. https://doi.org/10.1002/dmrr.3502
8. Guzik TJ, Nosalski R, Maffia P, Drummond GR (2024) Immune and inflammatory mechanisms in hypertension. Nat Rev Cardiol 21(6):396–416. https://doi.org/10.1038/s41569-023-00964-1
9. Filippi S, Vignozzi L, Morelli A et al (2009) Testosterone Partially Ameliorates Metabolic Profile and Erectile Responsiveness to PDE5 Inhibitors in an Animal Model of Male Metabolic Syndrome. J Sex Med 6(12):3274–3288. https://doi.org/10.1111/j.1743-6109.2009.01467.x
10. Maneschi E, Morelli A, Filippi S et al (2012) Testosterone treatment improves metabolic syndrome-induced adipose tissue derangements. J Endocrinol 215(3):347–362. https://doi.org/10.1530/JOE-12-0333
11. Vignozzi L, Filippi S, Comeglio P et al (2014) Nonalcoholic steatohepatitis as a novel player in metabolic syndrome-induced erectile dysfunction: An experimental study in the rabbit. Mol Cell Endocrinol 384(1–2):143–154. https://doi.org/10.1016/j.mce.2014.01.014
12. Comeglio P, Guarnieri G, Filippi S et al (2024) The galectin-3 inhibitor selvigaltin reduces liver inflammation and fibrosis in a high fat diet rabbit model of metabolic-associated steatohepatitis. Front Pharmacol 15:1430109. https://doi.org/10.3389/fphar.2024.1430109
13. Arias-Mutis OJ, Marrachelli VG, Ruiz-Saurí A et al (2017) Development and characterization of an experimental model of diet-induced metabolic syndrome in rabbit. Nadal A, ed. PLOS ONE 12(5):e0178315. https://doi.org/10.1371/journal.pone.0178315
14. Lozano WM, Arias-Mutis OJ, Calvo CJ, Chorro FJ, Zarzoso M (2019) Diet-Induced Rabbit Models for the Study of Metabolic Syndrome. Animals 9(7):463. https://doi.org/10.3390/ani9070463
15. Corona G, Rastrelli G, Vignozzi L et al (2021) The Role of testosterone treatment in patients with metabolic disorders. Expert Rev Clin Pharmacol 14(9):1091–1103. https://doi.org/10.1080/17512433.2021.1938548
16. Arias-Mutis ÓJ, Genovés P, Calvo CJ et al (2018) An Experimental Model of Diet-Induced Metabolic Syndrome in Rabbit: Methodological Considerations, Development, and Assessment. J Vis Exp 13457117. https://doi.org/10.3791/57117
17. Zhao S, Chu Y, Zhang C et al (2008) Diet-induced central obesity and insulin resistance in rabbits. J Anim Physiol Anim Nutr 92(1):105–111. https://doi.org/10.1111/j.1439-0396.2007.00723.x
18. Sarchielli E, Comeglio P, Filippi S et al (2020) Testosterone improves muscle fiber asset and exercise performance in a metabolic syndrome model. J Endocrinol 245(2):259–279. https://doi.org/10.1530/JOE-19-0532
19. De Falco M, Sciarrillo R, Capaldo A et al (2007) The Effects of the Fungicide Methyl Thiophanate on Adrenal Gland Morphophysiology of the Lizard, Podarcis sicula. Arch Environ Contam Toxicol 53(2):241–248. https://doi.org/10.1007/s00244-006-0204-2
20. Kleiner DE, Brunt EM, Van Natta M et al (2005) Design and validation of a histological scoring system for nonalcoholic fatty liver disease†. Hepatology 41(6):1313–1321. https://doi.org/10.1002/hep.20701
21. Comeglio P, Filippi S, Sarchielli E et al (2017) Anti-fibrotic effects of chronic treatment with the selective FXR agonist obeticholic acid in the bleomycin-induced rat model of pulmonary fibrosis. J Steroid Biochem Mol Biol 168:26–37. https://doi.org/10.1016/j.jsbmb.2017.01.010
22. Livak KJ, Schmittgen TD (2001) Analysis of Relative Gene Expression Data Using Real-Time Quantitative PCR and the 2−ΔΔCT Method. Methods 25(4):402–408. https://doi.org/10.1006/meth.2001.1262
23. Lis GJ, Jasek E, Litwin JA, Gajda M, Zarzecka J, Cichocki T (2010) Expression of basal cell marker revealed by RAM11 antibody during epithelial regeneration in rabbits. Folia Histochem Cytobiol 48(1):89–92. https://doi.org/10.2478/v10042-008-0087-3
24. Chan WK, Chuah KH, Rajaram RB, Lim LL, Ratnasingam J, Vethakkan SR (2023) Metabolic Dysfunction-Associated Steatotic Liver Disease (MASLD): A State-of-the-Art Review. J Obes Metab Syndr 32(3):197–213. https://doi.org/10.7570/jomes23052
25. Burstyn PG, Lloyd IJ, Horrobin DF (1971) Effects of progesterone on changes in arterial pressure following operation. Am J Obstet Gynecol 110(7):994–996. https://doi.org/10.1016/0002-9378(71)90555-2
26. Oddie CJ, Coghlan JP, Scoggins BA (1972) Plasma Deoxycorticosterone Levels in Man with Simultaneous Measurement of Aldosterone, Corticosterone, Cortisol and 11-Deoxycortisol. J Clin Endocrinol Metab 34(6):1039–1054. https://doi.org/10.1210/jcem-34-6-1039
27. White PC, Curnow KM, Pascoe L (1994) Disorders of Steroid 11β-Hydroxylase Isozymes*. Endocr Rev 15(4):421–438. https://doi.org/10.1210/edrv-15-4-421
28. Bulsari K, Falhammar H (2017) Clinical perspectives in congenital adrenal hyperplasia due to 11β-hydroxylase deficiency. Endocrine 55(1):19–36. https://doi.org/10.1007/s12020-016-1189-x
29. Sun B, Lu L, Gao Y et al (2022) High prevalence of hypertension and target organ damage in patients with 11β-hydroxylase deficiency. Clin Endocrinol (Oxf) 96(5):657–665. https://doi.org/10.1111/cen.14677
30. Tóth IE, Szabó D, Szalay KSz, Hesz Á (1990) Impaired Corticosteroid Production By Isolated Adrenocortical Cells Of Hypercholesterolemic Rabbits. Endocr Res 16(1):93–105. https://doi.org/10.1080/07435809009035922
31. Lee G, Kang K, Yun HH, Jo W, Oh T (2023) Multiple time-dependent pathophysiological changes in a rabbit model of high-fat diet-induced hyperlipidemia. FEBS Open Bio 13(6):1027–1040. https://doi.org/10.1002/2211-5463.13597
32. Swierczynska MM, Mateska I, Peitzsch M et al (2015) Changes in morphology and function of adrenal cortex in mice fed a high-fat diet. Int J Obes 39(2):321–330. https://doi.org/10.1038/ijo.2014.102